Picosecond Spin Seebeck Effect

Johannes Kimling,[1,*] Gyung-Min Choi,[2] Jack T. Brangham,[3] Tristan Matalla-Wagner,[4] Torsten Huebner,[4] Timo Kuschel,[4,5] Fengyuan Yang,[3] and David G. Cahill[1]

[1]*Department of Materials Science and Engineering and Materials Research Laboratory, University of Illinois, Urbana, Illinois 61801, USA*

[2]*Center for Spintronics, Korea Institute of Science and Technology, Seoul 136-791, Korea*

[3]*Department of Physics, The Ohio State University, 191 West Woodruff Avenue, Columbus, Ohio 43210, USA*

[4]*Center for Spinelectronic Materials and Devices, Department of Physics, Bielefeld University, Universitätsstrasse 25, 33615 Bielefeld, Germany*

[5]*Physics of Nanodevices, Zernike Institute for Advanced Materials, University of Groningen, Nijenborgh 4, 9747 AG Groningen, Netherlands*

(Received 25 July 2016; revised manuscript received 26 September 2016; published 1 February 2017)

We report time-resolved magneto-optic Kerr effect measurements of the longitudinal spin Seebeck effect in normal metal/$Y_3Fe_5O_{12}$ bilayers driven by an interfacial temperature difference between electrons and magnons. The measured time evolution of spin accumulation induced by laser excitation indicates transfer of angular momentum across normal metal/$Y_3Fe_5O_{12}$ interfaces on a picosecond time scale, too short for contributions from a bulk temperature gradient in an yttrium iron garnet. The product of spin-mixing conductance and the interfacial spin Seebeck coefficient determined is of the order of 10^8 $A\,m^{-2}\,K^{-1}$.

DOI: 10.1103/PhysRevLett.118.057201

I. Introduction.—Spin transport in magnetic insulators and through metal-insulator interfaces is extensively studied in the fields of spintronics and spincaloritronics, providing new routes for information technologies and heat-to-electricity conversion [1–3]. A key role in spin caloritronics is played by the longitudinal spin Seebeck effect (LSSE), which describes spin transport through the interface between a normal metal and a magnetic insulator upon heat transport through that interface [4].

The coupling between itinerant and localized electrons across the interface can be explained by an interfacial exchange interaction [5,6]. Based on this interaction, itinerant electrons scattering off the interface can create or annihilate magnons, thus allowing for interconversion of independent electron spin current in the normal metal and magnon spin current in the magnetic insulator. LSSE theories consider thermally excited spin currents in both directions across a metal/insulator interface: A spin current from insulator to metal driven by a thermal spin pumping mechanism, and a spin current from metal to insulator driven by random spin transfer torques [7–9]. In equilibrium, these opposite currents are equal. Application of a temperature gradient creates a net spin current that is proportional to the interfacial temperature difference between electrons and magnons. In addition to this interfacial LSSE, it has been proposed that a temperature gradient in the bulk of the insulator can drive spin transport by magnons. Depending on its direction, the temperature gradient can result in accumulation or depletion of magnons near the interface, enhancing or reducing the spin current from insulator to metal [10–13]. To date, isolation of interfacial LSSE from bulk LSSE has not been achieved experimentally.

Prior LSSE measurements are based on the inverse spin Hall effect (ISHE): the voltage signal measured is assumed to be caused by a spin current that has been converted into a transverse charge current. The symmetry of the resulting voltage signal with respect to the direction of the applied magnetic field is used as an indication of the ISHE. ISHE-based LSSE measurements have been reported for various insulators, e.g., ferrimagnetic garnets such as $Y_3Fe_5O_{12}$ (YIG) [14], Bi-substituted YIG [15], and $Gd_3Fe_5O_{12}$ [16], ferrimagnetic ferrites such as $NiFe_2O_4$ [17,18], $CoFe_2O_4$ [19,20], and Fe_3O_4 [21], as well as paramagnetic $Gd_3Ga_5O_{12}$ [22] and antiferromagnetic Cr_2O_3 [23] or MnF_2 [24]. The experiments are typically reported as observations of the LSSE. However, ISHE-based LSSE measurements are susceptible to unwanted voltage sources, e.g., proximity Nernst effects [25] and the conventional Seebeck effect driven by the thermal Hall heat current in the ferromagnetic layer [26]. Hence, independent LSSE measurements that are not based on the ISHE are desirable to corroborate the spin current hypothesis of the LSSE.

To date, time-resolved ISHE-based LSSE measurements have achieved a time resolution of the order of 1–100 ns [27,28]. Agrawal *et al.* investigate micrometer-thick YIG layers and report that the time scale of the LSSE is determined by the rise time of the temperature gradient in the YIG layer (~300 ns). They conclude that the LSSE is predominantly a bulk effect caused by magnon spin diffusion along the temperature gradient in the YIG layer. Based on this interpretation, they estimate a magnon spin diffusion length of ~500 nm for thermally excited magnons. Schreier *et al.* investigate YIG layers with thicknesses

between 50 nm and 30 μm applying heating frequencies up to ~1 GHz [28]. They measure roll-off frequencies of the LSSE that increase with decreasing YIG thickness. Schreier *et al.* attribute this roll-off to the finite magnon-phonon relaxation time in YIG and explain changes in the roll-off frequencies by assuming that the spectrum of magnons predominantly contributing to the LSSE shifts to higher frequencies when decreasing the YIG thickness. However, the roll-off frequencies for the different YIG thicknesses approximately match the thermal penetration depths in YIG at the respective frequencies, which supports the findings of Agrawal *et al.* discussed above.

Here, we present a LSSE experiment that is based on the time-resolved magneto-optic Kerr effect (TR-MOKE) and provides subpicosecond time resolution. Our experiment is not susceptible to spurious effects that often plague ISHE-based LSSE measurements. Taking advantage of the picosecond time scale, our experiment involves sizable temperature differences across Au/YIG and Cu/YIG interfaces, of the order of 10 to 100 K. The short time scale and the dominant temperature difference across the NM/YIG interface allow us to selectively probe the interfacial LSSE.

II. Experiment and model.—The samples are normal metal (NM)/YIG bilayers on $Gd_3Ga_5O_{12}$ (GGG) substrates with NM thicknesses between 35 and 103 nm and YIG thicknesses between 17 and 250 nm (compare Table I in the Supplemental Material [29]). We use Au and Cu as NM materials with long spin-relaxation times (1 order of magnitude longer compared to Pt) [30]. Moreover, Au and Cu exhibit small electronic heat capacities and weak electron-phonon coupling, which facilitate large electron temperature excursions during laser excitation.

The YIG of samples I through V was grown at Ohio State University by off-axis sputtering. The NM layers were grown by off-axis sputtering, for samples II and III *in situ* and for samples III through V *ex situ* after YIG deposition. References [31] and [32] demonstrate that the off-axis sputtered YIG thin films have a slightly larger off-axis lattice constant than bulk YIG, proper stoichiometry within the resolution of energy-dispersive x-ray spectroscopy, no apparent structural defects and impurities in areas examined by scanning transmission electron microscopy, interfacial roughness with Au less than 1 Å, a saturation magnetization significantly higher than for bulk YIG (~2100 compared to 1790 G), and a narrow ferromagnetic resonance in-plane linewidth (4.3 G at 9.61 GHz).

Samples VI through VIII were grown in collaboration between the University of Alabama and the University of Bielefeld, Germany. The YIG was deposited by pulsed-laser deposition. For samples VI and VII, Au was *ex situ* sputtered on as-grown YIG/GGG; for sample VIII, Cu was sputtered after vacuum annealing of YIG/GGG at 200 °C and 4.6×10^{-9} mbar for 1 h. The roughness of the NM/YIG interfaces from Alabama and Bielefeld is of the order of 5 Å, as determined using x-ray reflectivity.

In our measurements, done at the University of Illinois, the NM layer is excited with a train of optical pulses at a repetition rate of 80 MHz and absorbed fluences of ~1 J m^{-2} [29]. The laser energy is absorbed by electrons increasing the electron temperature and then transferred to phonons via electron-phonon scattering. To describe this heat transfer problem, we use a two-temperature model (2TM) of electrons and phonons,

$$C_e \frac{\partial T_e}{\partial t} - \Lambda_e \frac{\partial^2 T_e}{\partial x^2} = g_{ep}(T_p - T_e) + p(z,t), \quad (1)$$

$$C_p \frac{\partial T_p}{\partial t} - \Lambda_p \frac{\partial^2 T_p}{\partial x^2} = g_{ep}(T_e - T_p), \quad (2)$$

where C denotes volumetric heat capacity, Λ denotes thermal conductivity, g_{ep} is the coupling parameter between electrons (e) and phonons (p), and $p(z,t)$ is the optical absorption profile determined using a transfer matrix optical model [29]. We assume that the electronic heat capacity is proportional to the electron temperature, $C_e = \gamma_e T_e$, where γ_e is the electronic heat capacity coefficient. For Au and Cu, this low temperature approximation is valid for electron temperatures below ~1000 K [33].

The temperature excursion of electrons is of the order of 100 K during laser excitation (compare Fig. 1). After thermalization of electrons and phonons in the NM layer, the finite thermal conductance of the NM/YIG interface maintains a temperature difference between electrons and YIG phonons of the order of 10 K for ~100 picoseconds. Energy transfer across the NM/YIG interface is dominated by phonons. Energy transfer to YIG magnons can occur via direct coupling of electrons and magnons across the NM/YIG interface and through phonon-magnon coupling of YIG.

SSE theories predict that the temperature difference between YIG magnons and NM electrons drives a spin current across the NM/YIG interface [7–9],

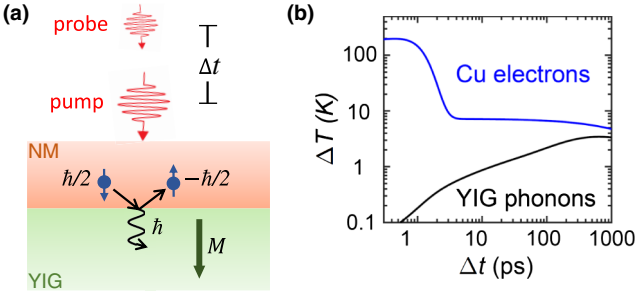

FIG. 1. Conceptual diagram and temperature transients. (a) Absorption of a pump laser pulse of picosecond duration generates a temperature difference between NM electrons and YIG magnons. Interfacial coupling between electrons and magnons induces spin accumulation in NM, which is probed by time-delayed probe laser pulses. (b) Example temperature transients of Cu electrons and YIG phonons calculated using the 2TM, Eqs. (1) and (2).

$$j_S = g_{\uparrow\downarrow}\frac{e^2}{h}S_S(T_e - T_m), \tag{3}$$

where $g_{\uparrow\downarrow}$ is the real part of the spin-mixing conductance per conductance quantum e^2/h and S_S is the interfacial spin Seebeck coefficient. Magnon heat capacity and phonon-magnon coupling parameter of YIG are unknown. Strong magnon-phonon coupling in YIG at room temperature has been conjectured by several authors [27,34–36]. Cornelissen *et al.* consider a magnon-phonon thermalization time of 0.1–1 picosecond [37]. Therefore, we approximate the magnon temperature by the phonon temperature of the YIG layer determined from the 2TM. In the results section below, we provide arguments that support the validity of this approximation.

During the pump-probe measurements, a magnetic field of ~0.4 T perpendicular to the sample plane rotates the YIG magnetization out of plane. If a significant amount of spin accumulation is generated in the NM layer, the resulting nonequilibrium magnetization rotates the polarization of light upon reflection [30]. We probe this polar Kerr effect with a train of sub-ps optical pulses at the same repetition rate of 80 MHz and a lower absorbed fluence of ~0.03 J m^{-2}. By varying the time delay between successive pump and probe pulses, we track rise and decay of spin accumulation subsequent to laser excitation [38]. To determine zero time delay and temporal heating profile, we use a GaP photodiode at the sample location, which measures the temporal profile of correlated pump and probe pulses by two-photon absorption. The magnitude of the polar Kerr signal for a given amount of spin accumulation is determined by the strength of spin-orbit coupling [30]. We use conversion factors between polar Kerr rotation and spin accumulation estimated in prior works (24×10^{-9} rad m A^{-1} for Au [30] and 4.5×10^{-9} rad m A^{-1} for Cu [38]). The Kerr rotation per magnetization unit is approximately five times larger for Au compared to Cu, due to stronger spin-orbit coupling in Au. A description of the experimental setup can be found in the Supplemental Material [29].

To describe spin accumulation in the NM layer, we consider the time-dependent spin diffusion equation

$$\frac{\partial\zeta_S}{\partial t} - D\frac{\partial^2\zeta_S}{\partial x^2} = \frac{\zeta_S}{\tau_S}, \tag{4}$$

and connect the spin current in Eq. (3) with the spin diffusion current $j_S = (\sigma/2e)[(\partial\zeta_S)/\partial x]$ at the NM/YIG interface. In the above equation, $\zeta_S = \zeta_\uparrow - \zeta_\downarrow$ is the difference of the chemical potentials of up and down spins, σ is the electrical conductivity, $D = \sigma/[e^2N(E_F)]$ is the diffusion constant of electrons, where $N(E_F)$ is the electronic density of states at the Fermi energy, and τ_S is the spin relaxation time. We fit the solution of the spin diffusion model to the measurement data using τ_S and the product $\alpha \equiv g_{\uparrow\downarrow}(e^2/h)S_S$ as free parameters (compare Fig. 2). Because of the large diffusion constant of electrons in Au and Cu, the spin accumulation created at the NM/YIG interface diffuses to the NM surface on a subpicosecond time scale. Hence, the spin accumulation near the NM surface varies by less than 1% across the optical penetration depth. Therefore, we assume that TR-MOKE measures the spin accumulation at the surface of the NM layer. The sensitivity of spin accumulation to α is a constant; the sensitivity of spin accumulation to τ_S peaks shortly after laser excitation, when the temperature excursion of the electrons falls back to the phonon temperature [29].

III. Results.—The measurement signal rises during laser excitation and decays to a plateau a few picoseconds after laser excitation (symbols in Fig. 2). The remaining signal decays slowly with the interfacial temperature difference for ~1 ns [29]. Solid lines in Fig. 2 are fit curves to the measurement data using the spin diffusion model described above. Since laser excitation initially creates a nonequilibrium state of the electrons that is not captured by the 2TM [39], we only fit decay and plateau of the measurement signal.

For the different Au/YIG samples, we obtain fit results for α that vary from $\sim3\times10^7$ to $\sim1\times10^8$ A m^{-2} K^{-1} and fit results for τ_S that vary from ~0.8 to ~1.7 ps; for the

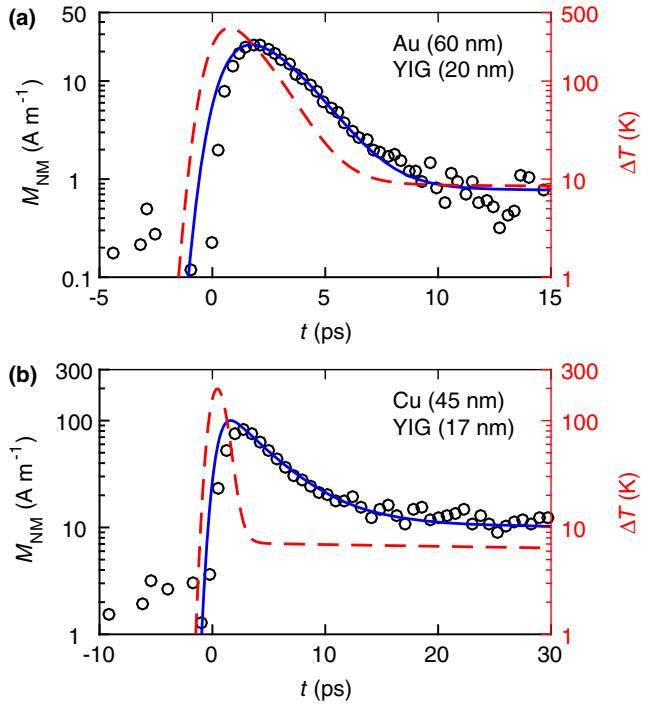

FIG. 2. Thermally induced spin accumulation in Au and Cu. TR-MOKE data (symbols) measured for two NM/YIG/GGG samples with layer thicknesses as stated in the figure. Solid lines show fit curves obtained using the spin diffusion model, Eqs. (3) and (4). Dashed lines show temperature excursion of electrons calculated using the 2TM, Eqs. (1) and (2). TR-MOKE data and fit curves for the other samples investigated are depicted in Fig. 2 of the Supplemental Material [29].

Cu/YIG sample from OSU, we obtain $\alpha = 3.4 \pm 1.2 \times 10^8$ A m^{-2} K^{-1} and $\tau_S = 3.7 \pm 0.8$ ps; for the Cu/YIG sample from Alabama and Bielefeld, we obtain $\alpha = 2.4 \pm 0.3 \times 10^8$ A m^{-2} K^{-1} and $\tau_S = 2.5 \pm 0.3$ ps. The errors were determined from contours of constant variance $\sigma^2 = 2\sigma^2_{\mathrm{fit}}$ between model prediction and measurement data in the two-dimensional parameter space of τ_S and S_S, where σ^2_{fit} is the variance when τ_S and S_S assume their fit values. Fit results for the individual samples are listed in Table I of the Supplemental Material [29], together with layer thicknesses determined from picosecond acoustics and x-ray reflectivity measurement, electrical conductivities determined from sheet resistivity measurements, and other model parameters including Refs. [40–49]. In the Supplemental Material [29], we also demonstrate that the Faraday effect in the microscope objective does not contribute to our measurement signals, show exemplary measurements that demonstrate a sign change for negative magnetic fields, and present reference measurements on a Au/glass sample that show no measurement signal [29].

Though the FWHM of the time correlation of pump and probe pulses is ~1.2 ps, the measurement signal does not rise before $t \approx 0$ ps. This delay cannot completely be explained by the finite diffusion time of spin and heat through the NM layer, which is considered in the model. The discrepancy between model and data during laser excitation could correspond to the characteristic time of the scattering processes involved. This characteristic time can be estimated using the time-energy-correlation $\Delta t \propto h/\Delta E$, where h is the Planck constant and ΔE is the interaction energy between electrons and magnons [50]. According to Ref. [13], magnon frequencies in YIG at 300 K are of the order of 5 THz. This gives a characteristic time of the interfacial scattering process of $\Delta t \approx 200$ fs, which is still a factor 2–3 too small for explaining the delayed rise of the measurement signal. However, recent SSE studies conjecture that predominantly low-frequency magnons (< 1 THz) contribute to the SSE [51–53], which could explain the delayed rise of the measurement signal. On the other hand, the discrepancy could also indicate that the 2TM fails in the subpicosecond time scale, where the electrons cannot be accurately described by a Fermi-Dirac distribution.

Good agreement between model and measurement signal over the fit range for different YIG thicknesses investigated and the finite measurement signal after electron-phonon thermalization in the NM layer support our assumption that the magnon temperature remains close to the phonon temperature. However, transfer of angular momentum across the NM/YIG interface is accompanied by energy transfer, which could lead to a reduction of the interfacial temperature difference between electrons and magnons. Therefore, we reanalyze the measurement data of the Au/YIG sample I considering a 2TM of magnons and phonons in the YIG layer. Based on the fit result $\alpha \approx 10^8$ A m^{-2} K^{-1} (compare Table I in the Supplemental Material [29]), we estimate an electron-magnon thermal conductance across the NM/YIG interface of $G_{em} = \alpha k_B T/(2e) \approx 10^6$ W m^{-2} K^{-1}. Assuming a magnetic heat capacity of YIG of $C_m = 1200$ J m^{-3} K^{-1}, theoretically calculated in Ref. [13], we estimate a minimum magnon-phonon coupling constant of $g_{\mathrm{mp}} \approx 3 \times 10^{14}$ W m^{-3} K^{-1}, required to obtain fit results within the error bars of the results obtained when setting the magnon temperature equal to the phonon temperature.

Explanation of our measurement signals in terms of bulk LSSE would require that a significant magnon temperature gradient develops in the YIG layer on a subpicosecond time scale. In our experiments, the YIG magnons are heated via heat transport across the NM/YIG interface. Because of the dominating heat capacity of phonons, subpicosecond fast heating of YIG magnons requires direct energy transfer between NM electrons and YIG magnons. As interfacial electron-magnon coupling needed for energy transfer simultaneously drives the interfacial LSSE, we can assume that bulk LSSE in our experiment presupposes the interfacial LSSE.

Indications on the significance of bulk LSSE can be achieved by varying the thickness of the YIG layer [28]. If present in our experiment, bulk LSSE would depend on the YIG thickness, if the length scale of magnon diffusion at the picosecond time scale exceeds the YIG thickness, and if magnon-phonon relaxation occurs on a time scale longer than the picosecond time scale. In that case, we expect that both interfacial LSSE and bulk LSSE increase with increasing YIG thickness due to the following reasoning: The interfacial LSSE increases with YIG thickness, because the additional magnon heat capacity decreases the rise of the magnon temperature and thus the interfacial temperature difference between electrons and magnons. The bulk LSSE also increases with YIG thickness, because the magnon temperature gradient in the YIG layer increases if the YIG thickness approaches or exceeds the length of magnon diffusion at the picosecond time scale. As the fit parameter α does not increase when changing the YIG thickness from 20 to 100 to 250 nm (sample I through sample IV), we draw the following conclusions: (1) The YIG magnon temperature remains close to the phonon temperature at the picosecond time scale; (2) contributions from bulk LSSE are negligible on picosecond time scales.

Variation of the Au thickness from 103 nm for sample VI to 29 nm for sample VII yields similar results for α. Since the 29-nm-thick Au layer is not completely opaque, this result indicates that light reflected in YIG and in GGG does not significantly contribute to the measurement signals in our experiment.

Using temperature-dependent measurements, we find that the fit parameter α decreases monotonically with temperature and vanishes approximately at the Curie temperature of YIG (compare Fig. 3). The measurement

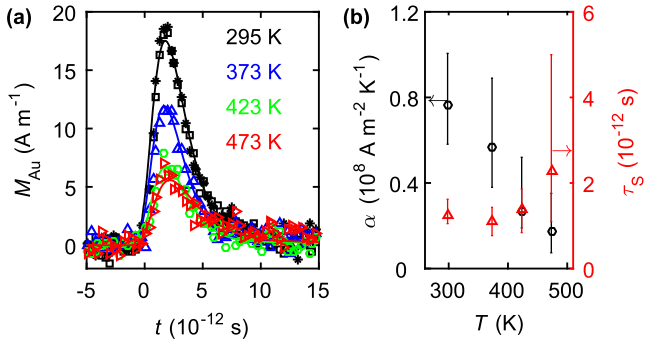

FIG. 3. Temperature-dependent measurements. (a) TR-MOKE data (symbols) measured on sample I at different temperatures as indicated. Solid lines show fit curves obtained using the spin diffusion model. (b) Fit results for $\alpha = g_{\uparrow\downarrow}e^2/hS_S$ (left y axis) and spin-relaxation time τ_S (right y axis) as a function of temperature.

signals before and after heating are reversible [compare open squares and asterisks in Fig. 3(a)]. The spin relaxation time does not show a significant temperature dependence within the error bars of our measurements. Fluence-dependent measurements indicate that the LSSE signal scales nonlinearly with the fluence, as expected based on the temperature coefficient of the electronic heat capacity (compare Fig. 10 in the Supplemental Material [29]).

Weiler *et al.* report ISHE-based LSSE measurements on Pt/Au/YIG/GGG and Pt/Cu/YIG/GGG samples assuming interfacial LSSE [54]. In their model that is based on the theory of Ref. [7], the parameter α is defined as

$$\tilde{\alpha} = \frac{g_{\uparrow\downarrow}\gamma e k_B}{\pi M_S V_a}, \tag{5}$$

where γ is the gyromagnetic ratio, k_B is the Boltzmann constant, M_S is the saturation magnetization, and V_a is the magnetic coherence volume. Weiler *et al.* experimentally determine a spin-mixing conductance of Au/YIG and Cu/YIG interfaces of $g_{\uparrow\downarrow} \approx 4 \times 10^{18}$ m^{-2}. Using Eq. (5) with $M_S = 140$ kA m^{-1} and $V_a = (1.3\ \text{nm})^3$ as reported by Weiler *et al.* [54], we obtain $\tilde{\alpha} \approx 16 \times 10^8$ A m^{-2} K^{-1}, which is 1 order of magnitude larger than our results. Note that the measurements of Weiler *et al.* include possible contributions from bulk LSSE.

IV. Conclusion.—Using a novel method that is not based on the ISHE, we achieved LSSE measurements at the picosecond time scale. Our experimental results corroborate LSSE theories that predict a spin current across the interface of a normal metal with a ferromagnetic insulator if magnons and electrons are out of equilibrium. We have isolated the interfacial LSSE and obtain a product of spin-mixing conductance and spin Seebeck coefficient of the order of 10^8 A m^{-2} K^{-1} for Au/YIG and Cu/YIG interfaces. Though our measurements indicate that the LSSE is active at the picosecond time scale, we find that the LSSE signal rises with a delay of 0.5 to 1 ps compared to our model prediction. To understand this delay, new LSSE theories are required that address the dynamics induced by subpicosecond laser pulses.

This work was carried out in part in the Frederick Seitz Materials Research Laboratory Central Research Facilities, University of Illinois. Financial support by the U.S. Army Research Office under Contract No. W911NF-14-1-0016, by the Deutsche Forschungsgemeinschaft [KI 1893/1-1 and KU 3271/1-1 (priority program Spin Caloric Transport, SPP 1538)], and by the Department of Energy (DOE), Office of Science, Basic Energy Sciences, under Award No. DE-SC0001304, is kindly acknowledged. We further thank Amit V. Singh, Zhong Li, and Arunava Gupta from the Center for Materials for Information Technology (MINT), Tuscaloosa, Alabama, as well as Alessia Niesen, Alexander Boehnke, and Günter Reiss from Bielefeld University, Germany, for assistance and discussion during sample preparation and for making available laboratory equipment. G. M. C. was supported by the National Research Council of Science & Technology (NST) grant (No. CAP-16-01-KIST) by the Korea government (MSIP).

*kimling@illinois.edu

[1] G. E. W. Bauer, E. Saitoh, and B. J. van Wees, Nat. Mater. **11**, 391 (2012).
[2] A. B. Cahaya, O. A. Tretiakov, and G. E. W. Bauer, IEEE Trans. Magn. **51**, 1 (2015).
[3] F. Hellman, A. Hoffmann, Y. Tserkovnyak, G. Beach, E. Fullerton, C. Leighton, A. MacDonald, D. Ralph, D. Arena, H. Durr *et al.*, arXiv:1607.00439.
[4] K. Uchida, H. Adachi, T. Ota, H. Nakayama, S. Maekawa, and E. Saitoh, Appl. Phys. Lett. **97**, 172505 (2010).
[5] S.-L. Zhang and S. Zhang, Phys. Rev. B **86**, 214424 (2012).
[6] S. A. Bender, R. A. Duine, and Y. Tserkovnyak, Phys. Rev. Lett. **108**, 246601 (2012).
[7] J. Xiao, G. E. W. Bauer, K. C. Uchida, E. Saitoh, and S. Maekawa, Phys. Rev. B **81**, 214418 (2010).
[8] H. Adachi, K. Uchida, E. Saitoh, and S. Maekawa, Rep. Prog. Phys. **76**, 036501 (2013).
[9] S. A. Bender and Y. Tserkovnyak, Phys. Rev. B **91**, 140402 (2015).
[10] S. D. Brechet, F. A. Vetro, E. Papa, S. E. Barnes, and J.-P. Ansermet, Phys. Rev. Lett. **111**, 087205 (2013).
[11] S. Hoffman, K. Sato, and Y. Tserkovnyak, Phys. Rev. B **88**, 064408 (2013).
[12] U. Ritzmann, D. Hinzke, and U. Nowak, Phys. Rev. B **89**, 024409 (2014).
[13] S. M. Rezende, R. L. Rodríguez-Suárez, R. O. Cunha, A. R. Rodrigues, F. L. A. Machado, G. A. Fonseca Guerra, J. C. Lopez Ortiz, and A. Azevedo, Phys. Rev. B **89**, 014416 (2014).
[14] K. Uchida, T. Nonaka, T. Kikkawa, Y. Kajiwara, and E. Saitoh, Phys. Rev. B **87**, 104412 (2013).

[15] G. Siegel, M. C. Prestgard, S. Teng, and A. Tiwari, Sci. Rep. **4**, 4429 (2014).
[16] S. Geprägs, A. Kehlberger, F. D. Coletta, Z. Qiu, E.-J. Guo, T. Schulz, C. Mix, S. Meyer, A. Kamra, M. Althammer *et al.*, Nat. Commun. **7**, 10452 (2016).
[17] D. Meier, T. Kuschel, L. Shen, A. Gupta, T. Kikkawa, K. Uchida, E. Saitoh, J.-M. Schmalhorst, and G. Reiss, Phys. Rev. B **87**, 054421 (2013).
[18] D. Meier, D. Reinhardt, M. van Straaten, C. Klewe, M. Althammer, M. Schreier, S. T. B. Goennenwein, A. Gupta, M. Schmid, C. H. Back *et al.*, Nat. Commun. **6**, 8211 (2015).
[19] T. Niizeki, T. Kikkawa, K.-i. Uchida, M. Oka, K. Z. Suzuki, H. Yanagihara, E. Kita, and E. Saitoh, AIP Adv. **5**, 053603 (2015).
[20] E.-J. Guo, J. Cramer, A. Kehlberger, C. A. Ferguson, D. A. MacLaren, G. Jakob, and M. Kläui, Phys. Rev. X **6**, 031012 (2016).
[21] R. Ramos, T. Kikkawa, M. H. Aguirre, I. Lucas, A. Anadón, T. Oyake, K. Uchida, H. Adachi, J. Shiomi, P. A. Algarabel *et al.*, Phys. Rev. B **92**, 220407 (2015).
[22] S. M. Wu, J. E. Pearson, and A. Bhattacharya, Phys. Rev. Lett. **114**, 186602 (2015).
[23] S. Seki, T. Ideue, M. Kubota, Y. Kozuka, R. Takagi, M. Nakamura, Y. Kaneko, M. Kawasaki, and Y. Tokura, Phys. Rev. Lett. **115**, 266601 (2015).
[24] S. M. Wu, W. Zhang, A. KC, P. Borisov, J. E. Pearson, J. S. Jiang, D. Lederman, A. Hoffmann, and A. Bhattacharya, Phys. Rev. Lett. **116**, 097204 (2016).
[25] S. Y. Huang, X. Fan, D. Qu, Y. P. Chen, W. G. Wang, J. Wu, T. Y. Chen, J. Q. Xiao, and C. L. Chien, Phys. Rev. Lett. **109**, 107204 (2012).
[26] J.-E. Wegrowe, H.-J. Drouhin, and D. Lacour, Phys. Rev. B **89**, 094409 (2014).
[27] M. Agrawal, V. I. Vasyuchka, A. A. Serga, A. Kirihara, P. Pirro, T. Langner, M. B. Jungfleisch, A. V. Chumak, E. T. Papaioannou, and B. Hillebrands, Phys. Rev. B **89**, 224414 (2014).
[28] M. Schreier, F. Kramer, H. Huebl, S. Geprägs, R. Gross, S. T. B. Goennenwein, T. Noack, T. Langner, A. A. Serga, B. Hillebrands *et al.*, Phys. Rev. B **93**, 224430 (2016).
[29] See Supplemental Material at http://link.aps.org/supplemental/10.1103/PhysRevLett.118.057201 for details on experimental setup, model parameters, measurement data, and fit curves for samples II through IV and samples VI through VIII, a discussion of through plane, in-plane, and temporal heating profiles, example sensitivity plots, a discussion of spurious signals, TR-MOKE measurements over longer time scales up to 500 ps, picosecond acoustic measurements, and fluence-dependent TR-MOKE measurements.
[30] G.-M. Choi and D. G. Cahill, Phys. Rev. B **90**, 214432 (2014).
[31] J. C. Gallagher, A. S. Yang, J. T. Brangham, B. D. Esser, S. P. White, M. R. Page, K.-Y. Meng, S. Yu, R. Adur, W. Ruane *et al.*, Appl. Phys. Lett. **109**, 072401 (2016).
[32] J. T. Brangham, K.-Y. Meng, A. S. Yang, J. C. Gallagher, B. D. Esser, S. P. White, S. Yu, D. W. McComb, P. C. Hammel, and F. Yang, Phys. Rev. B **94**, 054418 (2016).
[33] Z. Lin, L. V. Zhigilei, and V. Celli, Phys. Rev. B **77**, 075133 (2008).
[34] M. Schreier, A. Kamra, M. Weiler, J. Xiao, G. E. W. Bauer, R. Gross, and S. T. B. Goennenwein, Phys. Rev. B **88**, 094410 (2013).
[35] N. Roschewsky, M. Schreier, A. Kamra, F. Schade, K. Ganzhorn, S. Meyer, H. Huebl, S. Geprägs, R. Gross, and S. T. B. Goennenwein, Appl. Phys. Lett. **104**, 202410 (2014).
[36] J. Flipse, F. K. Dejene, D. Wagenaar, G. E. W. Bauer, J. B. Youssef, and B. J. van Wees, Phys. Rev. Lett. **113**, 027601 (2014).
[37] L. J. Cornelissen, K. J. H. Peters, G. E. W. Bauer, R. A. Duine, and B. J. van Wees, Phys. Rev. B **94**, 014412 (2016).
[38] G.-M. Choi, C.-H. Moon, B.-C. Min, K.-J. Lee, and D. G. Cahill, Nat. Phys. **11**, 576 (2015).
[39] G. Tas and H. J. Maris, Phys. Rev. B **49**, 15046 (1994).
[40] M. N. Polyanskiy, "Refractive index database", http://refractiveindex.info.
[41] G. B. Scott, D. E. Lacklison, and J. L. Page, Phys. Rev. B **10**, 971 (1974).
[42] D. L. Wood and K. Nassau, Appl. Opt. **29**, 3704 (1990).
[43] Y. S. Touloukian and E. H. Buyco, *Thermophysical Properties of Matter*, The TPRC Data Series Vol. 4 (IFI/Plenum, New York, 1971).
[44] A. Tari, *The Specific Heat of Matter at Low Temperatures* (Imperial College Press, London, 2003).
[45] R. B. Wilson, B. A. Apgar, W.-P. Hsieh, L. W. Martin, and D. G. Cahill, Phys. Rev. B **91**, 115414 (2015).
[46] G. Tas, J. J. Loomis, H. J. Maris, A. A. Bailes, and L. E. Seiberling, Appl. Phys. Lett. **72**, 2235 (1998).
[47] A. E. Clark and R. E. Strakna, J. Appl. Phys. **32**, 1172 (1961).
[48] A. M. Hofmeister, Phys. Chem. Miner. **33**, 45 (2006).
[49] M. Krzesinska and T. Szuta-Buchacz, Phys. Status Solidi **82**, 421 (1984).
[50] E. Carpene, H. Hedayat, F. Boschini, and C. Dallera, Phys. Rev. B **91**, 174414 (2015).
[51] S. R. Boona and J. P. Heremans, Phys. Rev. B **90**, 064421 (2014).
[52] H. Jin, S. R. Boona, Z. Yang, R. C. Myers, and J. P. Heremans, Phys. Rev. B **92**, 054436 (2015).
[53] T. Kikkawa, K.-i. Uchida, S. Daimon, Z. Qiu, Y. Shiomi, and E. Saitoh, Phys. Rev. B **92**, 064413 (2015).
[54] M. Weiler, M. Althammer, M. Schreier, J. Lotze, M. Pernpeintner, S. Meyer, H. Huebl, R. Gross, A. Kamra, J. Xiao *et al.*, Phys. Rev. Lett. **111**, 176601 (2013).